International Journal of Hydrogen Energy 96 (2024) 763–770

Contents lists available at ScienceDirect

International Journal of Hydrogen Energy

journal homepage: www.elsevier.com/locate/he

Low frequency quartz tuning fork as hydrogen sensor

Chaofan Feng [a,b,c,1], Andrea Zifarelli [c,1], Giansergio Menduni [c], Angelo Sampaolo [a,b,c,d], Hongpeng Wu [a,b,***], Lei Dong [a,b], Vincenzo Spagnolo [a,b,c,d,*], Pietro Patimisco [a,b,c,d,**]

[a] State Key Laboratory of Quantum Optics and Quantum Optics Devices, Institute of Laser Spectroscopy, Shanxi University, Taiyuan, 030006, China
[b] Collaborative Innovation Center of Extreme Optics, Shanxi University, Taiyuan, 030006, China
[c] PolySense Lab—Dipartimento Interateneo di Fisica, University and Politecnico of Bari, Bari, Italy
[d] PolySense Innovations Srl, Bari, Italy

ARTICLE INFO

Handling Editor: Dr M Mahdi Najafpour

Keywords:
Hydrogen sensor
Quartz tuning fork
Piezoelectric resonator
Beat-frequency detection

ABSTRACT

The use of hydrogen as a sustainable energy source is pushing the development of innovative sensing strategies for the monitoring of H_2 concentration during its production processes and transportation. In this work, we propose a custom quartz tuning fork (QTF) as sensor for the detection of high concentrations of hydrogen in air. The selectivity derives directly from values of molar mass and the viscosity of hydrogen molecules, significantly different from those of the other main constituents of air. Exciting the fundamental flexural mode of a commercially available 12.4 kHz-QTF, we demonstrated the linear dependence of its resonance frequency and quality factor on the H_2 concentration, passing through their relationship with molar mass and the viscosity of the H_2-air mixture. Monitoring the shift of the resonance frequency of the QTF, the H_2-component in air can be estimated with a precision level of 0.74% and accuracy error of 1.82%. The same parameters resulted 0.40% and 4.29%, respectively, when Q values are evaluated. Finally, a beat-frequency approach was proposed to speed up the acquisition in few seconds, monitoring both resonance parameters of the QTF.

1. Introduction

In the realm of sustainable energy, hydrogen offers a clean, efficient, and versatile solution to the world's pressing environmental challenges. This is a huge incentive for scientific community, which is making giant efforts towards the deep understanding of the principles governing hydrogen production and utilization, as well as to promote innovative technologies for its storage and transport. The development of cutting-edge sensing technology for monitoring the quality of the entire H_2 production process, together with its numerous subprocesses, constitutes a key part of the general framework. The demands for an ideal hydrogen sensor include: a highly sensitive dynamic detection within a concentration range up to 100%, high accuracy, sensitivity, and selectivity against reducing gases like NH_3, CO and H_2S, as well as fast response and recovery time. Other important requirements such as explosion proof capability, long-term stability and low-cost are highly desirable.

Currently, commercially available sensors for hydrogen detection are electrical sensors, namely thermal conduction sensors, catalytic sensors, semiconducting metal oxide-based resistive sensors, and electrochemical sensors [1–3]. However, these devices strongly suffer electromagnetic interferences; moreover, possible sparks in the mixture can cause uncontrolled explosions due to high inflammability of hydrogen at high concentrations. Conversely, detection of H_2 with optical techniques can guarantee the immunity to electromagnetic interferences. They are divided in two classes: hydride-based optical hydrogen sensors and

* Corresponding author. State Key Laboratory of Quantum Optics and Quantum Optics Devices, Institute of Laser Spectroscopy, Shanxi University, Taiyuan, 030006, China.
** Corresponding author. State Key Laboratory of Quantum Optics and Quantum Optics Devices, Institute of Laser Spectroscopy, Shanxi University, Taiyuan, 030006, China.
*** Corresponding author. State Key Laboratory of Quantum Optics and Quantum Optics Devices, Institute of Laser Spectroscopy, Shanxi University, Taiyuan, 030006, China.
E-mail addresses: wuhp@sxu.edu.cn (H. Wu), vincenzoluigi.spagnolo@poliba.it (V. Spagnolo), pietro.patimisco@uniba.it (P. Patimisco).
[1] These authors equally contributed to the presented work

https://doi.org/10.1016/j.ijhydene.2024.11.365
Received 1 October 2024; Received in revised form 18 November 2024; Accepted 21 November 2024
Available online 27 November 2024

tunable diode laser absorption spectroscopy (TDLAS) sensors. The first type exploits the capability of some metals to absorb hydrogen and in turn form metal hydrides [4]. Due to their small size, H_2 atoms can easily fit and occupy the interstitial sites of the lattice to form metal hydrides, causing both a volume expansion and a change of the permittivity, that can be monitored by optical detection systems. For example, in fiber grating sensors the metal hydride is deposited on the cladding: the exposition to hydrogen will generate an expansion and consequently a mechanical stress that will vary the grating period, resulting in the wavelength shift of the light at the fiber exit [5,6]. Alternatively, interferometer sensing systems, including the Mach-Zehnder [7,8], the Fabry-Perot [9,10] and the Sagnac interferometer [11], are used to detect variations of both the refractive index and the size of the metal hydride when exposed to H_2. Palladium is the most used material for hydride-based optical hydrogen sensors due to its high capability of hydrogen absorption. However, the short lifetime, the low response rate, the long recovery time, the low stability, and the influence of humidity have slowed down the large-scale use and commercialization of hydride-based optical hydrogen sensors [2]. Moreover, this class of sensors is not suitable for exposures at high hydrogen concentrations: they are specifically designed to operate below the explosive limit of hydrogen (4%) to prevent their damage; only a few works go beyond this limit. However, there are many cases, hydrogen fuel cells for instance, which makes it necessary to measure hydrogen at high concentrations.

TDLAS is based on the optical absorption of hydrogen molecules when they are irradiated by a laser spectrally tuned to be resonant to a radiative molecular transition. A TDLAS scheme is composed by a laser source, an absorption cell containing the hydrogen mixture and a photodetector for measuring the laser power transmitted by the cell after the optical absorption. By correlating it with the incident power, the Lambert-Beer law allows a calibrated measurement of the hydrogen concentration within the gas cell. The main drawback is that the molecular hydrogen is a diatomic homonuclear molecule, with no dipole moment: therefore, H_2 exhibits limited, very weak vibrational lines related to quadrupole transitions. This imposes a strict limitation on the choice of a laser source: all TDLAS hydrogen sensors reported in literature use a distributed-feedback diode laser to target the H_2 quadrupole absorption line at 2121.8 nm. Thereby, to compensate the weak absorption cross-section, TDLAS hydrogen sensors exploits long absorption pathlengths [12], or multi-pass absorption cells to increase the sensitivity [13], and sophisticated fitting algorithm for denoising [14]. W. Ye also reported on an optical gas sensor for hydrogen and water detection based on photoacoustic spectroscopy [15]. In addition to optical techniques, acoustic hydrogen sensors have been proposed, based on the detection of changes in the properties of acoustic waves due to an adsorbate deposited on the surface of a piezoelectric material. Also in these cases, metal hydrides are used as sensitive element deposited on piezoelectric substrates. Hydrogen concentrations can be retrieved by monitoring changes in the acoustic wave propagation due to the absorption of hydrogen molecules by palladium, namely the resonance frequency, the mass loading, and the propagation time of the acoustic waves for quartz crystal microbalance sensor [16], surface acoustic wave sensor [17] and acoustic sensor based on sound velocity measurements [18], respectively. Being mass sensitive, acoustic sensors are highly susceptible to interference from other gases, including water vapor, as well as to variations in temperature that affect the sound velocity.

In this work, we propose a commercially available acoustic detection module, composed by a quartz tuning fork (QTF) and a transimpedance amplifier, for the measurement of the hydrogen concentration in a standard air. The principle of detection is based on the high sensitivity of the resonance properties of a quartz tuning fork (QTF) on the variation of molar mass and the viscosity of the gas mixture while the QTF is vibrating at its fundamental flexural mode. Compared to the components of standard air, both parameters are significantly different for the hydrogen molecules, which is a key feature to ensure a high specificity and a wide range of detection. Previous works reported in literature exploited the change of resonant properties of modified piezoelectric resonators with functionalized coatings, such as polymers [19,20]. However, the fabrication procedure, the fragility of the employed structures, and the already mentioned narrow operative concentration range prevents their use for hydrogen detection. Conversely, the proposed solution represents a solid and reliable alternative for high-concentration hydrogen sensing.

2. Effect of the gas properties on the flexural vibrational mode of a QTF

The resonance properties of a quartz tuning fork (QTF) vibrating at the fundamental flexural mode are highly sensitive to the variability of the environmental conditions, such as temperature, pressure, humidity, gas viscosity and gas density. Consequently, the resonance frequency and the quality factor of the vibrational mode experiences sudden variations, that can be individually quantified and related to the cause.

2.1. The natural frequency

The natural frequencies of a QTF submerged in a gaseous medium differ from those in vacuum. This can be easily intended as an effect of gas forces on the submerged QTF prongs, represented as an additional inertia to the vibration, which decreases the natural frequencies of the prongs from those which would be measured in the vacuum. The governing partial differential equation for the dynamic deflection of the prong is based on the Euler–Bernoulli (E-B) beam theory. When the prong is vibrating inside a gaseous medium, the E-B includes the additional inertia of the prong as an added mass because, conceptually speaking, it must move some volume of surrounding gas as it vibrates through it. Thus, the E-B equation can be used to calculate the effect of the added mass on natural frequencies and modes shape of the fluid-beam coupled system. Assuming that each prong of a QTF is a vibrating beam that can be treated separately, the E-B equation of motion for the transverse deflection of a prong, ignoring shear deformation and rotary inertia effects, can be written in the form [21]:

$$EI\frac{\partial^4 y(x,t)}{\partial x^4} + (\rho A + u)\frac{\partial^2 y(x,t)}{\partial t^2} = 0 \tag{1}$$

where $y(x,t)$ is the lateral deflection at distance x along the length of the beam, EI, ρ, A and u are the flexural rigidity, the quartz density, the cross-sectional area of the prongs and the added mass, respectively. The added mass is incorporated into the E-B equation by considering an effective linear mass (the term in the round brackets) as the sum of the linear mass ρA of the prong and the added mass per unit length. By imposing the clamped-free boundary conditions, the natural frequencies can be retrieved [22]:

$$f = f_0 - \frac{1}{2}\frac{f_0 u}{\rho A} \tag{2}$$

where f_0 is the natural frequency when $u = 0$, i.e., in vacuum. The natural frequency decreases linearly with the added mass. Being the added mass related to the gas moved while the prong is vibrating, a simple formulation of the added mass suggests a proportionality with the gas density ρ_g. In the ideal gas low approximation, the gas density can be related to the pressure P:

$$\rho_g = \frac{M_g P}{RT} \tag{3}$$

where M_g, R and T are the molar mass, the gas constant and the temperature, respectively.

2.2. The quality factor

The quality factor of a vibrating prong represents its energy efficiency and therefore it is linked to its dissipation mechanisms. This implies that as the stored energy decreases due to the dissipation, the loss increases. The viscous damping is the dominant factor of dissipation for a prong in gaseous environments. Therefore, the overall quality factor Q can be represented as the sum of two contributions [23]:

$$\frac{1}{Q}=\frac{1}{Q_0}+\frac{1}{Q_g} \tag{4}$$

where Q_g is related only to the gas damping, and Q_0 includes all other loss mechanisms not influenced by the surrounding gas medium (usually it includes the support loss and the thermoelastic damping). Hosaka et al. [24] proposed an approach for the modeling of the viscous effects by extending the Landau's model and representing the cantilever beam as a string of spheres, resulting in the following equation to determine Q_g:

$$\frac{1}{Q_g}=\frac{3\pi\mu+\frac{3}{4}\pi w\sqrt{4\pi\rho_g\mu f}}{4\pi\rho A f} \tag{5}$$

where μ is the gas viscosity and w is the prong width. As before, the gas density can be related with the pressure by using Eq. (3), explaining the dependence of the quality factor by the pressure and the viscosity of the surrounding gaseous medium.

3. Experimental setup

The acoustic detection module used for hydrogen detection is the ADM01 available on Thorlabs GmbH catalogue [25], designed as the sensing module for the quartz-enhanced photoacoustic spectroscopy (QEPAS) [26]. The ADM01 module has an inlet and outlet allowing the gas flow to be injected into the airtight chamber, which contains a spectrophone composed by a custom QTF acoustically coupled with a pair of resonator tubes. The QTF has T-shaped prongs properly designed to resonate at ~12.45 kHz at the fundamental flexural mode with a quality factor >12,000 at atmospheric pressure, in standard air [27]. The two tubes, placed on the V-groove of a cylinder and located on both sides of the QTF, are used to probe and amplify the acoustic wave generated within the ADM01 via photoacoustic effect, when it is used in QEPAS sensors. The acoustic coupling between the two tubes has been extensively studied in terms of the spatial distribution of the sound wave pattern, probed by the QTF placed between them [28]. The analytical model predicts a strong dependence of the acoustic coupling on the tube diameter and the wavenumber of the sound wave in the tubes 2πf/v, being v the speed velocity in the gas mixture. Dealing with H_2:N_2 mixtures, the sound speed of the mixture varies from 354 m/s to 1320 m/s when the concentration of molecular hydrogen changes from 0 to 100%. This huge variability of the wavenumber is reflected on the acoustic coupling between tubes, and in turn on the quality factor of the spectrophone. Therefore, it will compete with the gas damping mechanism (discussed in Section 2.2) on altering the resonance properties of the spectrophone, when the H_2 concentration varies in the test mixture. To avoid unpredictable behavior hard to be modelled and interpreted, we decided to remove tubes from ADM01 and use the bare QTF. The H_2 sensor based on the modified version of the ADM01 is sketched in Fig. 1.

The fundamental flexural mode of the QTF is excited exploiting the inverse piezoelectric effect on quartz crystal. A waveform generator (Tektronix AFG 3102) is used to provide a sinusoidal voltage excitation to the QTF, resulting in a piezoelectric charge distribution across the QTF prongs. Charges are collected by gold electrodes deposited on QTF prongs and the piezoelectric current is then converted to sinusoidal voltage signal by means of the transimpedance preamplifier mounted under the ADM01. The output voltage is sent to a digital lock-in

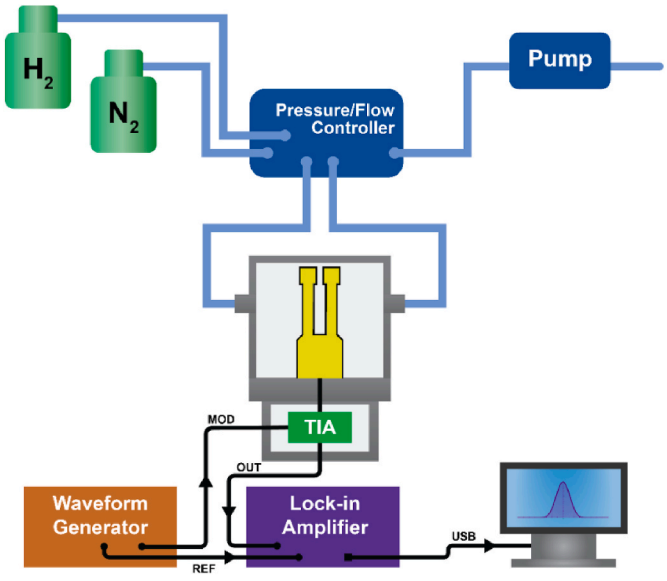

Fig. 1. Sketch for the experimental apparatus for hydrogen sensing. TIA, transimpedance preamplifier; MOD, input modulation; OUT, QTF output signal; REF, reference signal.

amplifier (MFLI, Zurich Instruments), which is used to demodulate the signal at the same frequency of the sinusoidal excitation. The resonance curve of the QTF is reconstructed by varying step-by-step the frequency of the waveform generator (with an excitation peak-to-peak voltage of 20 mV) and acquiring the 1f lock-in amplifier signal.

The gas handling system for the H_2 sensor calibration consists of two cylinders of pure N_2 and pure H_2, respectively, entering the gas blender (MCQ-Instruments GM VACUUM 1.3) for the generation of mixtures at different H_2:N_2 concentrations upstream the modified ADM01. The same instrument was used to regulate the gas pressure in the chamber in the range between 50 and 760 torr, at a constant flow of 100 sccm.

4. Characterization of the QTF in one-component samples

The effect of the hydrogen on both resonance frequency and the quality factor of the fundamental mode of the QTF can be discussed by analyzing their trends as a function of the pressure, with respect to the standard case of nitrogen in the ADM. With the above-mentioned assumption of $u\propto\rho_g$, the combination of Eqs. (2) and (3) leads to a linear dependence of the resonance frequency as a function of the pressure:

$$f=f_0-kP \tag{6}$$

with k dependent on the molar mass of the mixture. By combining Eqs. (4) and (5), the dependence of the overall quality factor by the pressure can be rewritten as:

$$\frac{1}{Q(P)}=A+B\sqrt{P} \tag{7}$$

with

$$A=\frac{3\pi\mu}{4\pi\rho A f}+\frac{1}{Q_0} \tag{8}$$

and

$$B=\frac{\frac{3}{4}\pi w\sqrt{4\pi\frac{M_{gas}}{RT}\mu f}}{4\pi\rho A f} \tag{9}$$

The resonance curve of the QTF was acquired at different pressure

values, first when the QTF is immersed in pure N_2, and then in pure H_2. Each spectral curve was fitted by using a Lorentzian function to determine the resonance frequency, corresponding to the peak value, and the full-width-half-maximum (FWHM) of the fit function. The FWHM was used to determine the Q-factor measured as the ratio between the peak value and the FWHM for the resonance curve. The extracted resonance frequencies and the calculated 1/Q values for both H_2 and N_2 are plotted as a function of the pressure in Fig. 2a and b, respectively. The uncertainties associated to the extracted fit parameters are covered by the experimental points.

The resonance frequency shows a linear behavior ($R^2 > 0.95$) as a function of the pressure for both N_2 and H_2. The two intercept values, 12456.39 Hz for N_2 and 12456.56 Hz for H_2, differs from each other, although the E-B model predicts a common value f_0, i.e., the natural frequency in vacuum. This discrepancy is expected because it exists a critical pressure below which the ideal gas law approximation is no longer valid: the gas enters in the molecular regime and damping mechanisms are caused by independent collisions of non-interacting molecules with the vibrating prong. In this regime, the gas loses its characteristics as ideal medium [29]. As a result, below the critical pressure (not reached in the presented analysis), the pressure-trend of the resonance frequency will deviate from a linear behavior. From the linear fit, a slope of $k_{N2} = -1.011$ mHz/Torr and $k_{H2} = -0.110$ mHz/Torr was extracted for N_2 and H_2, respectively. The ratio k_{N2}/k_{H2} results 9.2 and, according to Eq. (2) with the approximation $u \propto \rho_g$, it should be equal to the ratio between the molar mass of the nitrogen ($M_{N2} = 28$) and the molar mass of the hydrogen ($M_{H2} = 2$), resulting 14. The inaccuracy of the calculated value with respect to expected one is strongly affected by the approximation done on the modeling of the added mass, which can be considered as an oversimplification. Methods of determining the total hydrodynamic force on a vibrating beam are more complicated and based on combination of empirical, experimental, and theoretical procedures, which is beyond the scope of this work [30]. Equation (7) was used to fit the 1/Q experimental values, as shown in Fig. 2b. The fitting procedure returns $B_{N2} = 2.57{\cdot}10^{-6}$ Torr$^{-1/2}$ and $B_{H2} = 0.59{\cdot}10^{-6}$ Torr$^{-1/2}$ for N_2 and H_2, respectively, whose ratio is $B_{N2}/B_{H2} = 4.36$. Equation (9) shows a dependence of B-parameter on the square root of the product between the molar mass and the viscosity of the gas. Assuming $\mu_{N2} = 17.3$ μPa s and $\mu_{H2} = 8.7$ μPa s as the dynamic viscosity of molecular nitrogen and hydrogen, respectively, the ratio B_{N2}/B_{H2} between the expected values results 5.28, in good agreement with the experimental results (inaccuracy of 17%), confirming the robustness of the Hosaka' approach in modeling the air damping mechanism for an oscillating beam.

5. Measurement of H_2 concentration in N_2-matrix

Fig. 2a and b suggest that the effect of the hydrogen on the resonance properties of the QTF are more prominent at higher pressures, with respect to the resonance curves acquired in pure molecular nitrogen. Therefore, all the measurements of H_2 in N_2-matrix presented hereafter were performed at 700 Torr. When the QTF is immersed in a mixture containing a x hydrogen mole fraction and nitrogen as rest, an effective molar mass of the mixture can be defined by multiplying the molar mass of N_2 and H_2 in the mixture by its relative amount and then adding them together:

$$M_{eff} = xM_{H2} + (1-x)M_{N2} = x(M_{H2} - M_{N2}) + M_{N2} \tag{10}$$

By including Eq. (10) in Eq. (6), a linear dependence of the resonance frequency on the hydrogen concentration with a positive slope can be predicted (because $M_{H2} < M_{N2}$), provided that the gas mixture pressure is kept constant.

For the quality factor trend, the effective viscosity is involved, as shown in Eqs. (7)–(9). For a binary ideal mixture with viscosities μ_{H2} and μ_{N2}, meaning that the components do not produce any change in volume, the dynamic effective viscosity, μ_{eff}, obeys the Arrhenius equation [31]:

$$\ln \mu_{eff} = x\ln\mu_{H2} + (1-x)\ln \mu_{N2} \tag{11}$$

After a few mathematical steps, it is easy to demonstrate that:

$$\mu_{eff} \propto e^{x(\ln \mu_{H2} - \ln \mu_{N2})} \tag{12}$$

with exponent negative since $\ln \mu_{H2} < \ln \mu_{N2}$. Making explicit the minus sign and considering that the domain field of the variable x is [0,1], the exponential function can be linearized in first approximation as:

$$\mu_{eff} \propto 1 - x|\ln \mu_{H2} - \ln \mu_{N2}| \tag{13}$$

Combining Eqs. (7)–(9) with Eqs. (10) and (12), and highlighting only the dependence on the effective molar mass and the effective dynamic viscosity, meaning that all other multiplying parameters are grouped as constant, the quality factor trend as a function of the hydrogen mole fraction can be written as:

$$\frac{1}{Q(P)} \propto \frac{1}{Q_0} + C(1 - x|\ln \mu_{H2} - \ln \mu_{N2}|) + D\sqrt{(1 - x|\ln \mu_{H2} - \ln \mu_{N2}|)\left(1 - x\left|\frac{M_{H2} - M_{N2}}{M_{N2}}\right|\right)} \tag{14}$$

It can be easily verified that as a first approximation:

$$|\ln \mu_{H2} - \ln \mu_{N2}| \approx \left|\frac{M_{H2} - M_{N2}}{M_{N2}}\right| \approx 1 \tag{15}$$

and the 1/Q trend as a function of the hydrogen mole fraction can be easily linearized with a negative slope.

With the experimental setup depicted in Fig. 1, different mixtures of H_2:N_2 were generated by using the gas blender, starting from two cylinders with pure H_2 and N_2. The resonance curves of the QTF were acquired at different H_2 mole fraction. Fig. 3a and b report the resonance

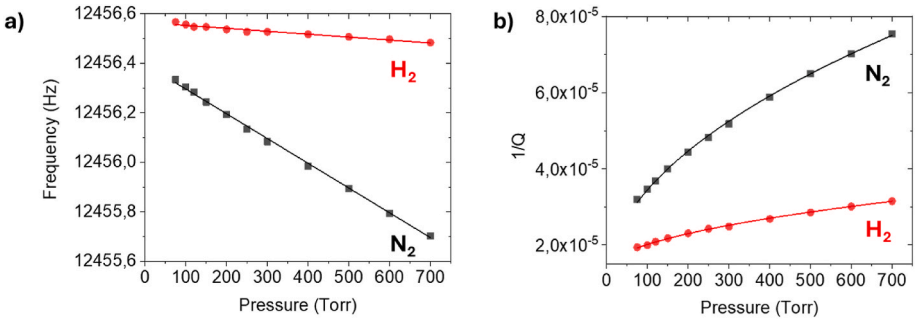

Fig. 2. Resonance frequency (a) and 1/Q (b) values at different pressures, in pure N_2 (black squares) and in pure H_2 (red dots). The solid lines represent the best fit of experimental data by using Eq. 6(a) and Eq. 7(b). (For interpretation of the references to colour in this figure legend, the reader is referred to the Web version of this article.)

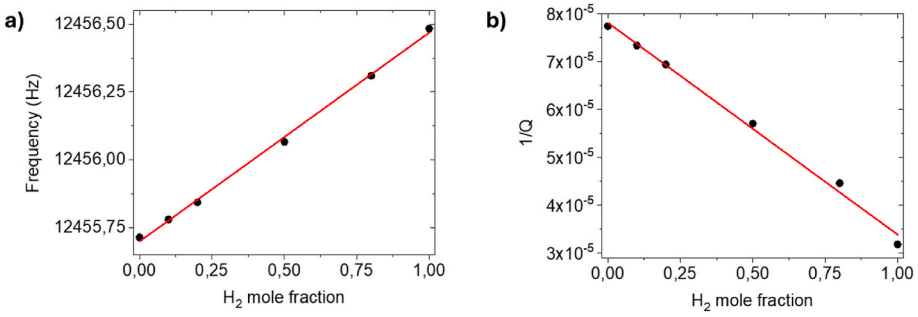

Fig. 3. Experimental data (black dots) and linear fit (red curve) of the resonance frequency (a) and 1/Q values (b) extracted from the Lorentzian fit of the QTF resonance curves at different H_2 mole fractions. All the measurements were performed at 700 Torr. (For interpretation of the references to colour in this figure legend, the reader is referred to the Web version of this article.)

frequency and the 1/Q values as a function of the hydrogen mole fraction, respectively.

Both resonance parameters follow a linear trend as a function of the hydrogen mole fraction, as predicted by the theoretical modeling, also with the right sign of the slope. It is only noteworthy that the datapoints at 0.8 and 1.0 hydrogen mole fraction slightly deviates from the linear fit, which conversely well fit the other datapoints. This is an expected consequence of the linearization imposed in Eq. (12), which can be considered strictly feasible for hydrogen mole fraction values sufficiently lower than the unit. Table 1 summarizes the parameters extracting from the linear fits.

Both fit functions are considered as calibration curves to retrieve the hydrogen concentration in gas mixtures, with the chance to use the resonance frequency or 1/Q as sensor response.

To evaluate the ultimate performances of the QTF-based hydrogen detection, two metrics must be estimated, namely the precision and the accuracy. The first one is specified as the standard deviation, i.e., the square root of the statistically estimated variance of a series of independent measurements of the resonance frequency and the quality factor. To build the dataset, for each hydrogen concentration used in the calibration curves (Fig. 3a and b), the resonance curve of the QTF was measured 50 times in series, with a deadtime of 5 s between two consecutive curve acquisitions. For each resonance curve, the frequency and 1/Q-values were extracted as before and plotted as a function of the number of the measurement, separately, for evaluating the 1σ standard deviation and the mean value of the two datasets. As representative, the resonance frequency and the 1/Q-value extracted for 50 consecutive measurements are plotted in Fig. 4, when pure nitrogen flows in the ADM.

For the other mixtures, similar 1σ-values were found, with a discrepancy less than 1% each other. Therefore, the precision for hydrogen detection can be estimated as the ratio between the standard deviation and the sensitivity, i.e., the slope of the calibration curve in Table 1, resulting in 7.40 mmol fraction when the resonance frequency is used as sensor response, corresponding to 0.74% concentration in volume. With the same procedure, a precision level of 40.2 mmol fraction was estimated taken 1/Q as sensor response, corresponding to a ~0.40% concentration in volume.

The accuracy of the sensor is estimated as the largest deviation from the ideal H_2 concentration, given by the input mixtures used during the calibration, of the H_2 concentration calculated from the calibration curve using the mean values of the datasets. When the resonance

Table 1
Slope and Intercept of the linear fits for the resonance frequency and the 1/Q values at different hydrogen mole fractions.

	Slope	Intercept
Resonance frequency	0.770 Hz/(mole fraction)	12455.699 Hz
1/Q	$-4.427 \cdot 10^{-5}$ (mole fraction)$^{-1}$	$7.813 \cdot 10^{-5}$

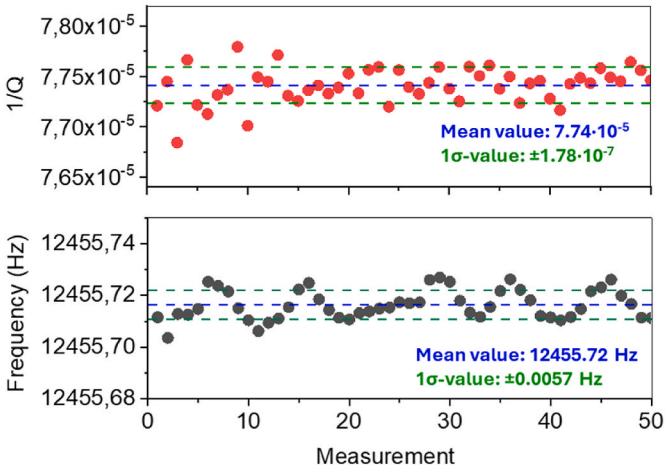

Fig. 4. 1/Q (upper panel) and resonance frequency (lower panel) values extracted from the Lorentzian fit of 50 QTF resonance curves, acquired in pure nitrogen.

frequency is used as sensor response, the largest deviation estimated is 0.014 Hz, resulting in an accuracy error of 1.82% concentration in volume; when the 1/Q value is used, the highest deviation is $1.90 \cdot 10^{-6}$, resulting in an accuracy error of 4.29% concentration in volume. Such a large deviation is expected because the 1/Q values at high hydrogen concentrations deviate from the calibration curve (see Fig. 2b) because of the approximation used in the theoretical model, as already discussed.

Finally, the H_2 QTF-based sensor was calibrated by diluting H_2 with laboratory standard air, as a proof-of-concept for outdoor operation. The air sample is taken from the laboratory environment, reflecting typical atmospheric composition: nitrogen (~77%), oxygen (~21%), water vapor (~1.2%), CO_2 (~400 ppm), and trace species (below 5 ppm). Following the same procedure for dilution with N_2, a calibration curve for the resonance frequency and for 1/Q-values was extracted and plotted as a function of the H_2 concentration in Fig. 5a and b, together with the data of Fig. 3a and b, respectively, for ease of comparison.

Although the binary mixture N_2/H_2 is significantly different from the complex mixture H_2/air, only slight variations of the sensor performance have been recorded. This is attributed to the minimal differences in molar mass (from 28.02 to 28.96 g/mol) and viscosity (from 18.2 to 17.3 μPa s) between nitrogen and air. In detail, the increase of slope for the resonance frequency curve calibration is attributed to the linear dependence of slope on the effective molar mass of the mixture, as shown in Eq. (10). This effect is less pronounced for the 1/Q-trend because in this case the slope (see Eq. (13)) has a dependence on the square root of the effective molar mass; moreover, the viscosity of air (18.2 μPa s) is quite comparable with that of molecular hydrogen (17.3 μPa s). It can be immediately assumed that small variations in the

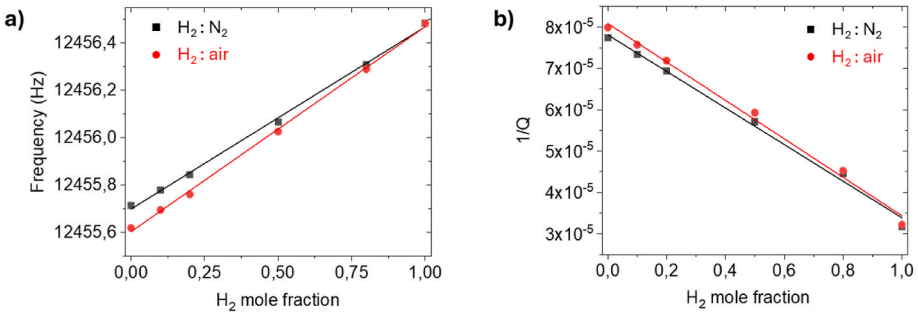

Fig. 5. a) Resonance frequency in N_2 (black squares) and in air (red dots) and b) 1/Q values in N_2 (black squares) and in air (red dots) extracted from the Lorentzian fit of the QTF resonance curves and measured at different H_2 mole fractions. All the measurements were performed at 700 Torr. (For interpretation of the references to colour in this figure legend, the reader is referred to the Web version of this article.)

concentrations of individual components in the air sample cannot significantly impact the sensor's performance in detecting H_2 in the air.

6. Beat frequency approach

The H_2 detection described so far takes ~1 min for the full scan of the resonance curve of the QTF to extract its FWHM and peak value. A different approach can be used to speed up the acquisition, called as beat-frequency (B–F), already validated in QEPAS techniques for the fast monitoring of the QTF resonance properties [32–34]. In the B–F approach reported in this paper, the QTF is excited for ~0.1 s with a sinewave at a modulation frequency f_B that is Δf-detuned with respect to the natural frequency f. As the sinewave pulse is completed, the QTF will relax and oscillate at its natural frequency. Being the QTF signal demodulated at f_B, the lock-in output in time-domain will show up as a damped sinusoidal waveform at the beat frequency Δf. The time coordinate of each peak can be extracted and fitted with the exponential law $e^{-t/\tau}$. The estimated τ value and the time intervals Δt between two consecutive peaks will return the quality factor of the QTF as $Q = \pi\tau f$ and its resonance frequency as $f = f_B \pm 1/\Delta t = f_B \pm \Delta f$, respectively [30]. The same setup depicted in Fig. 1 was used to optimize the B–F signal in terms of f_B and the results are reported in Fig. 6a, together with the QTF resonance curve of the fundamental mode, at 700 Torr when pure N_2 flows in the ADM01.

The B–F QTF signal (black squares) has two symmetric sidelobes detuned of $\Delta f = \pm 2.6$ Hz with respect to the peak value of the QTF resonance curve (red dots). The right and left lobes are perfectly symmetric; therefore the choice of the modulation frequency is completely arbitrary. We decided to set $f_B = f - \Delta f = 12453.1$ Hz. Fig. 6b reports the B–F signal as a function of the time (black solid line) acquired at the conditions described before, with a lock-in time constant of 5 ms to accurately sample the fast response. The dotted green line is the best fit of the red dots by using the function $e^{-t/\tau}$, as already discussed. The B–F approach allowed a reduction of the acquisition time down to less than 3 s, with respect to the ~ 1-min-long measurement of the standard approach described in the previous section. Then, the B–F QTF signal was acquired at different H_2 concentrations in N_2; the resonance frequency and the quality factor of the QTF were extracted and plotted as a function of the H_2 concentration in Fig. 7a and b, respectively.

The sensitivity of the QTF-based H_2 sensor operating in B–F approach is 0.722 Hz/(mole fraction) and $-4492 \cdot 10^{-5}$ (mole fraction)$^{-1}$ when the resonance frequency and the quality factor is used as sensor response, respectively. Both calibration curves are strongly consistent with those obtained when the QTF-based H_2 sensor operates in standard approach, as can be easily inferred with a comparison with the data listed in Table 1.

7. Conclusion

This work proposes a sensor for H_2 detection in air which operates by monitoring the resonance properties of a quartz tuning fork. It exploits the significant differences of the molar mass and the viscosity of the molecular hydrogen with respect to other components in air. The sensing element was assembled starting from a detection module already available on the market, without the need for new production processes. This can be expected to impact positively on the final cost of the sensor, especially in a perspective of large-scale production. Together with a high sensing performance, a QTF-based H_2 sensor overcomes the weaknesses of other technologies. Indeed, it offers: i) immunity of electromagnetic interferences, as a direct consequence of dielectric properties of the quartz crystal; ii) negligible risk for possible sparks in the mixture, because the fundamental mode can be excited with weak electric field and the preamplifier is located outside the airtight chamber; iii) response time of few seconds, if the B–F approach is adopted; iv) negligible recovery time, because the resonator accumulation time is < 1 s; v) capability to detect hydrogen concentrations

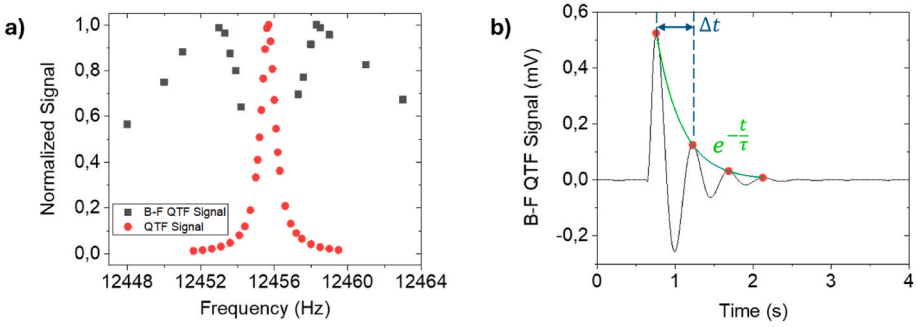

Fig. 6. a) Normalized response (red dots) and B–F signal (black squares) of the QTF at 700 Torr in N_2 as a function of the modulation frequency. b) Optimized B–F signal measured with $f_B = 12453.1$ Hz, at 700 Torr in N_2. Red circles highlight the peak values employed for the measurement of the Δt (dashed light blue lines) and the τ (dotted green line). (For interpretation of the references to colour in this figure legend, the reader is referred to the Web version of this article.)

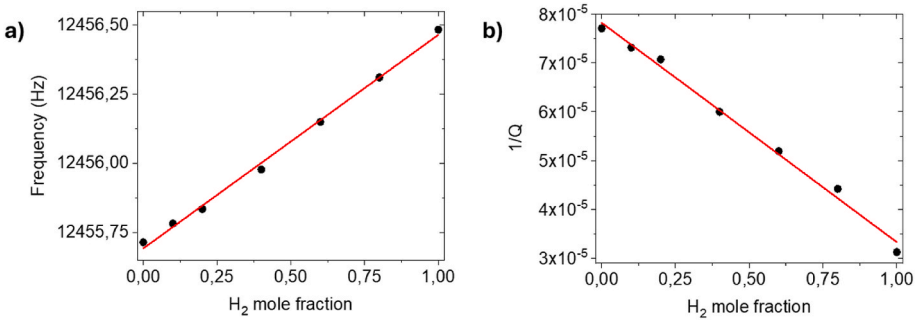

Fig. 7. Experimental data (black dots) and linear fit (red curve) of the a) resonance frequency and b) 1/Q values extracted from the analysis of the B–F QTF signal at different H_2 mole fractions. (For interpretation of the references to colour in this figure legend, the reader is referred to the Web version of this article.)

up to 100% without damage the sensing element. The physics underlying the sensing mechanism can be easily extended to other binary gas mixtures. The ultimate sensitivity is primarily determined by the difference in molar mass and/or viscosity between the two components: the greater this difference, the better the sensor's performance. Moreover, future improvements can be easily adopted. For example, a PTH (Pressure, Temperature and Relative Humidity) sensor can be easily integrated in the airtight chamber for mapping the influence of sensor H_2 sensitivity on atmospheric parameters, to extend the functionality of the sensor to other environments as well. In addition, the ultimate performance can be increased by processing both the resonance properties, i.e., the frequency and the quality factor, moving to univariate to multivariate calibration by a covariance measure of the similarity of the two parameters. This approach would address the main drawback of the proposed method, namely the lack of sensitivity when dealing with complex gas mixtures, where multiple components may undergo significant changes in concentrations simultaneously. Finally, the same QTF can be employed in a TDLAS setup as a photodetector [14], enabling the simultaneous detection of hydrogen and other impurities coming from the H_2 production processes.

CRediT authorship contribution statement

Chaofan Feng: Investigation, Formal analysis, Data curation. **Andrea Zifarelli:** Writing – review & editing, Writing – original draft, Supervision, Methodology, Formal analysis, Data curation. **Giansergio Menduni:** Writing – review & editing, Supervision, Investigation, Formal analysis, Data curation, Conceptualization. **Angelo Sampaolo:** Writing – review & editing, Supervision, Methodology, Data curation. **Hongpeng Wu:** Writing – review & editing, Validation, Supervision. **Lei Dong:** Writing – review & editing, Validation, Supervision. **Vincenzo Spagnolo:** Writing – review & editing, Validation, Supervision, Methodology, Funding acquisition. **Pietro Patimisco:** Writing – review & editing, Writing – original draft, Methodology, Formal analysis, Data curation, Conceptualization.

Declaration of competing interest

The authors declare that they have no known competing financial interests or personal relationships that could have appeared to influence the work reported in this paper.

Acknowledgements

The authors from Dipartimento Interateneo di Fisica di Bari acknowledge financial support from PNRR MUR project PE0000023-NQSTI and MUR project – Dipartimenti di Eccellenza 2023–2027 – Quantum Sensing and Modeling for One-Health (QuaSiModO). Andrea Zifarelli and Pietro Patimisco acknowledge financial support from the project "HIGAS - Development of a Hydrogen Impurity Gas Analyzer based on quartz-enhanced photoacoustic Spectroscopy" (D33C22001330002) within the framework of PNRR MUR project PE0000021-NEST - Network 4 Energy Sustainable Transition.

References

[1] Hübert T, Boon-Brett L, Black G, Banach U. Hydrogen sensors – a review. Sensor Actuator B Chem 2011;157:329–52. https://doi.org/10.1016/J.SNB.2011.04.070.
[2] Korotcenkov G, Han S Do, Stetter JR. Review of electrochemical hydrogen sensors. Chem Rev 2009;109:1402–33. https://doi.org/10.1021/CR800339K/ASSET/IMAGES/MEDIUM/CR-2008-00339K_0039.GIF.
[3] Boon-Brett L, Bousek J, Black G, Moretto P, Castello P, Hübert T, et al. Identifying performance gaps in hydrogen safety sensor technology for automotive and stationary applications. Int J Hydrogen Energy 2010;35:373–84. https://doi.org/10.1016/J.IJHYDENE.2009.10.064.
[4] Chen K, Yuan D, Zhao Y. Review of optical hydrogen sensors based on metal hydrides: recent developments and challenges. Opt Laser Technol 2021;137:106808. https://doi.org/10.1016/J.OPTLASTEC.2020.106808.
[5] Sutapun B, Tabib-Azar M, Kazemi A. Pd-coated elastooptic fiber optic Bragg grating sensors for multiplexed hydrogen sensing. Sensor Actuator B Chem 1999;60:27–34. https://doi.org/10.1016/S0925-4005(99)00240-3.
[6] Ma GM, Li CR, Luo YT, Mu RD, Wang L. High sensitive and reliable fiber Bragg grating hydrogen sensor for fault detection of power transformer. Sensor Actuator B Chem 2012;169:195–8. https://doi.org/10.1016/J.SNB.2012.04.066.
[7] Butler MA. Optical fiber hydrogen sensor. Appl Phys Lett 1984;45:1007–9. https://doi.org/10.1063/1.95060.
[8] Wang M, Yang M, Cheng J, Dai J, Yang M, Wang DN. Femtosecond laser fabricated micro Mach-Zehnder interferometer with Pd film as sensing materials for hydrogen sensing. Opt Lett 2012;37:1940. https://doi.org/10.1364/OL.37.001940.
[9] Wang M, Yang M, Cheng J, Zhang G, Liao CR, Wang DN. Fabry-pérot interferometer sensor fabricated by femtosecond laser for hydrogen sensing. IEEE Photon Technol Lett 2013;25:713–6. https://doi.org/10.1109/LPT.2013.2241421.
[10] Zhou X, Ma F, Ling H, Yu B, Peng W, Yu Q. A compact hydrogen sensor based on the fiber-optic Fabry-Perot interferometer. Opt Laser Technol 2020;124:105995. https://doi.org/10.1016/J.OPTLASTEC.2019.105995.
[11] Yang F, Gong H, Yang M, Wang DN, Xu B, Zhao CL, et al. Sagnac interferometer hydrogen sensor based on panda fiber with Pt-loaded WO_3/SiO_2 coating. Opt Lett 2016;41(7):1594–7. https://doi.org/10.1364/OL.41.001594. 41:1594–7.
[12] Avetisov V, Bjoroey O, Wang J, Geiser P, Paulsen KG. Hydrogen sensor based on tunable diode laser absorption spectroscopy. Sensors 2019;19:5313. https://doi.org/10.3390/S19235313. 2019;19:5313.
[13] Liang T, Qiao S, Liu X, Ma Y. Highly sensitive hydrogen sensing based on tunable diode laser absorption spectroscopy with a 2.1 μm diode laser. Chemosensors 2022;10:321. https://doi.org/10.3390/CHEMOSENSORS10080321. 2022;10:321.
[14] Ma Y, Liang T, Qiao S, Liu X, Lang Z. Highly sensitive and fast hydrogen detection based on light-induced thermoelastic spectroscopy. Ultrafast Science 2023;3. https://doi.org/10.34133/ULTRAFASTSCIENCE.0024/ASSET/72B6307E-6918-4329-9639-7615115BF2F1/ASSETS/GRAPHIC/ULTRAFASTSCIENCE.0024.FIG.010.JPG.
[15] Ye W, Xia Z, He L, Huang Y, Liu W, Luo W, et al. Photoacoustic dual-gas sensor for simultaneous detection of hydrogen and water vapor. Int J Hydrogen Energy 2023;48:20124–32. https://doi.org/10.1016/J.IJHYDENE.2023.01.374.
[16] Dong S, Bai F, Li JF, Viehland D. Sound-resonance hydrogen sensor. Appl Phys Lett 2003;82:4590–2. https://doi.org/10.1063/1.1586994.
[17] Huang FC, Chen YY, Wu TT. A room temperature surface acoustic wave hydrogen sensor with Pt coated ZnO nanorods. Nanotechnology 2009;20. https://doi.org/10.1088/0957-4484/20/6/065501.
[18] Vyas JC, Katti VR, Gupta SK, Yakhmi JV. A non-invasive ultrasonic gas sensor for binary gas mixtures. Sensor Actuator B Chem 2006;115:28–32. https://doi.org/10.1016/J.SNB.2005.08.016.
[19] Sampson SA, Date KS, Panchal SV, Ambrale A, Datar SS. Investigation of QTF based gas sensors. Sensor Actuator B Chem 2015;216:586–94. https://doi.org/10.1016/J.SNB.2015.04.024.

[20] Yun M, Lee S, Yim C, Jung N, Thundat T, Jeon S. Suspended polymer nanobridge on a quartz resonator. Appl Phys Lett 2013;103. https://doi.org/10.1063/1.4817259/667652.
[21] Christen M. Air and gas damping of quartz tuning forks. Sensor Actuator 1983;4:555–64. https://doi.org/10.1016/0250-6874(83)85067-7.
[22] Patimisco P, Borri S, Sampaolo A, Beere HE, Ritchie DA, Vitiello MS, et al. A quartz enhanced photo-acoustic gas sensor based on a custom tuning fork and a terahertz quantum cascade laser. Analyst 2014;139:2079–87. https://doi.org/10.1039/C3AN01219K.
[23] Patimisco P, Sampaolo A, Mackowiak V, Rossmadl H, Cable A, Tittel FK, et al. Loss mechanisms determining the quality factors in quartz tuning forks vibrating at the fundamental and first overtone modes. IEEE Trans Ultrason Ferroelectrics Freq Control 2018;65:1951–7. https://doi.org/10.1109/TUFFC.2018.2853404.
[24] Hosaka H, Itao K, Kuroda S. Damping characteristics of beam-shaped micro-oscillators. Sens Actuators A Phys 1995;49:87–95. https://doi.org/10.1016/0924-4247(95)01003-J.
[25] THORLABS ADM01 https://www.thorlabs.com/newgrouppage9.cfm?objectgroup_id=2940 n.d. https://www.thorlabs.com/newgrouppage9.cfm?objectgroup_id=2940.
[26] Patimisco P, Sampaolo A, Dong L, Tittel FK, Spagnolo V. Recent advances in quartz enhanced photoacoustic sensing. Appl Phys Rev 2018;5:011106. https://doi.org/10.1063/1.5013612.
[27] Patimisco P, Sampaolo A, Giglio M, Dello Russo S, Mackowiak V, Rossmadl H, et al. Tuning forks with optimized geometries for quartz-enhanced photoacoustic spectroscopy. Opt Express 2019;27:1401. https://doi.org/10.1364/oe.27.001401.
[28] Dello Russo S, Giglio M, Sampaolo A, Patimisco P, Menduni G, Wu H, et al. Acoustic coupling between resonator tubes in quartz-enhanced photoacoustic spectrophones employing a large prong spacing tuning fork. Sensors 2019;19. https://doi.org/10.3390/s19194109.
[29] Giglio M, Menduni G, Patimisco P, Sampaolo A, Elefante A, Passaro VMN, et al. Damping mechanisms of piezoelectric quartz tuning forks employed in photoacoustic spectroscopy for trace gas sensing. Phys Status Solidi (A) Appl Mater Sci 2019;216:1800552. https://doi.org/10.1002/pssa.201800552.
[30] Nuriev A, Kamalutdinov A, Zaitseva O, Affane B. Evaluation of drag and added mass forces acting on vibrating cantilever beams in the air. MATEC Web of Conf 2018;211:11004. https://doi.org/10.1051/MATECCONF/201821111004.
[31] Grunberg L, Nissan AH. Mixture law for viscosity. Nature 1949;164. https://doi.org/10.1038/164799b0. 4175 1949;164:799–800.
[32] Wu H, Dong L, Zheng H, Yu Y, Ma W, Zhang L, et al. Beat frequency quartz-enhanced photoacoustic spectroscopy for fast and calibration-free continuous trace-gas monitoring. Nat Commun 2017;8(1):1–8. https://doi.org/10.1038/ncomms15331. 2017;8.
[33] Li B, Menduni G, Giglio M, Patimisco P, Sampaolo A, Zifarelli A, et al. Quartz-enhanced photoacoustic spectroscopy (QEPAS) and Beat Frequency-QEPAS techniques for air pollutants detection: a comparison in terms of sensitivity and acquisition time. Photoacoustics 2023;31:100479. https://doi.org/10.1016/j.pacs.2023.100479.
[34] Rousseau R, Maurin N, Trzpil W, Bahriz M, Vicet A. Quartz tuning fork resonance tracking and application in quartz enhanced photoacoustics spectroscopy. Sensors 2019;19:5565. https://doi.org/10.3390/S19245565. 2019;19:5565.